Journal of Alloys and Compounds 514 (2012) 189–194

Contents lists available at SciVerse ScienceDirect

Journal of Alloys and Compounds

journal homepage: www.elsevier.com/locate/jallcom

Comparison of the behavior of Zr(41.2%)Ti(13.8%)Cu(12.5%)Ni(10%)Be(22.5%) amorphous and crystallized mirrors under deuterium ion bombardment

Alexandra F. Bardamid[a], Vladimir S. Voitsenya[b,*], James W. Davis[c], Vladimir G. Konovalov[b], Konstantin V. Kovtun[b], Ivan V. Ryzhkov[b], Anatoly F. Shtan'[b], Sergei I. Solodovchenko[b], Oleg V. Trembach[b], Andrei A. Vasil'ev[b], Uwe Breuer[d], Andrey Litnovsky[e]

[a] Taras Shevchenko National University, 01033 Kiev, Ukraine
[b] National Science Center "KIPT", 61108 Kharkov, Ukraine
[c] University of Toronto Institute for Aerospace Studies, 4925 Dufferin St., Toronto, ON, Canada M3H5T6
[d] Zentralabteilung für Chemische Analysen, Forschungszentrum Jülich, D-52425 Jülich, Germany
[e] Institut für Plasmaphysik, Association EURATOM, TEC, FZ-Jülich, Germany

ARTICLE INFO

Article history:
Received 21 September 2011
Received in revised form 31 October 2011
Accepted 11 November 2011
Available online 22 November 2011

Keywords:
Bulk metallic glasses
Mirrors
Deuterium plasma ions
Deuterium absorption
Destruction

ABSTRACT

Experiments have been performed to determine the effect of deuterium plasma exposure on mirrors fabricated from $Zr_{41.2}Ti_{13.8}Cu_{12.5}Ni_{10}Be_{22.5}$ alloy (Vitraloy 1, V1) in both the amorphous and crystallized state. It was found that for deuterium ion fluences above $\sim 2.6 \times 10^{24}$ ions/m^2, cracks and chips appeared on the surface of the crystallized mirrors. At a factor of two higher fluence, 5.2×10^{24} ions/m^2 of 60 eV ions, one specimen disintegrated into many fragments. The mirror specimens kept in the amorphous state, however, were not observed to have experienced any visual changes even after exposure to ion fluences as high as 1.5×10^{25} ions/m^2. The difference in behaviour is explained as being due to hydrogen embrittlement, and differences in hydrogen transport between the two alloy states.

1. Introduction

Bulk amorphous glasses (BAGs) including amorphous metal alloys (AMAs) have been the subject of experimental study for nearly two decades [1,2]. More recently, they are beginning to find practical uses in applications where there is a need to have materials with unique properties [3,4]. Among the most promising AMAs are alloys based on zirconium [5–7], as they possess a low critical cooling rate, which allows for the production of moldings of a sufficiently large size. At the same time, it has been found that specimens fabricated from these alloys have become brittle after saturation with hydrogen [8], a property common to other Zr-alloys [9].

Due to their high fracture toughness and hardness, and good homogeneity (e.g. [4]), BAGs may find useful application as mirrors in situations requiring dimensional stability and the maintenance of surface quality under extreme conditions. Metallic mirrors are integral parts of many plasma diagnostic systems in current and future fusion devices [10]. When such mirrors are located in erosion (as opposed to deposition) zones in a tokamak, they may be eroded due to bombardment by charge-exchange atoms (D°, T°, He°) with a wide energy distribution [11]. In previous papers [12–14], we have reported the results of investigations of the surface morphology and optical properties of mirrors fabricated from the amorphous alloy $Zr_{41.2}Ti_{13.8}Cu_{12.5}Ni_{10}Be_{22.5}$. Those experiments were intended to model the behavior of mirrors in the ITER tokamak. The mirror specimens were exposed to ions from deuterium and argon plasmas, but to limited ion fluences. In the current paper, we have extended the ion fluence range to further investigate the hydrogen embrittlement properties of this AMA.

2. Experiment

2.1. $Zr_{41.2}Ti_{13.8}Cu_{12.5}Ni_{10}Be_{22.5}$ materials

The starting point for specimen preparation was the casting of billets from the constituent metals. The primary metal components had purities >99.9 wt% and the melting procedure was done in an arc smelting chamber with a nonconsumable electrode inside the cavity of a water-cooled copper mould. The shape and size of the billets was determined by the shape of the cavity, and the quantity of material used. Typical size and weights for the billets were 25–28 mm diameter, 12–14 mm thick, and weight ~25 g. Electroerosion machining was used to cut individual specimens from the billets. Each billet was cut into two disc specimens with diameter 22 mm, thickness ~4 mm and weight ~8.5 g. One of each pair of discs was annealed in vacuum at 773 K for 1 h in order to transform the amorphous structure into a

* Corresponding author. Tel.: +380 57 3356437; fax: +380 57 3352664.
E-mail address: voitseny@ipp.kharkov.ua (V.S. Voitsenya).

0925-8388/$ – see front matter © 2011 Elsevier B.V. All rights reserved.
doi:10.1016/j.jallcom.2011.11.062

Table 1
Weight loss of the crystallized specimen AMC-1 measured following exposure to ions of Ar and D plasmas.

Exposure number	Working gas	Ion energy (eV)	Exposure time (min); (ion fluence, 10^{23} ions/m^2)	Mass loss (μg)
1	Ar	200 eV	60 (3.17)	1970
2	Ar	500 eV	15 (0.74)	1195
3	Ar	1000 eV	5 (0.35)	980
4	D_2	1000 eV	20 (1.57)	0
5	D_2	1000 eV	30 (2.35)	20
6	D_2	1000 eV	30 (2.35)	130
7	D_2	1000 eV	30 (2.35)	560
8	D_2	1000 eV	40 (3.14)	265
9	D_2	60 eV	180 (14.1)	2900 (Chips, see. Fig. 2)

fine crystalline structure; the transition was demonstrated by means of an X-ray diffractometer. One surface of each specimen was ground and polished with gradual decrease of the abrasive grit size to a high quality mirror finish. The use of mirror pairs cut from the same billet insures a direct comparison between the behavior of the amorphous and crystallized specimens when exposed to deuterium plasmas.

2.2. Plasma ion exposure

Plasma exposures were carried out in the DSM-2 facility described in Ref. [15]. Mirror specimens were exposed to ions extracted from a deuterium plasma (in some cases from an argon plasma) by applying a negative potential to a water-cooled copper specimen holder. Typical plasma parameters for the electron-cyclotron resonance (ECR) plasmas were $T_e \approx 5$ eV and $n_e \approx 10^{16}$ m^{-3}. The accelerating voltage could be varied in the range 40–1500 V, and the exposure times varied from 5 to 60 min for Ar plasmas, and 20–1760 min for D plasmas. After each exposure, specimens were weighed with an accuracy of 25 μg, and the spectral reflectance (wavelengths: 220–650 nm) was measured ex situ. As a rule, for deuterium ion energies below 1000 eV a mass gain was observed, despite evidence for sputtering for ion energies ≥300 eV [14]. Some specimens were also subjected to laser ablation to measure the D content in the ablated layers.

3. Results

Fig. 1 (reproduced from Ref. [13]) shows the results of X-ray diffractometer measurements for one pair of specimens (AMA-0 and AMC-0). The relative intensity of X-ray reflections for the unannealed specimen (AMA-0) has a characteristic diffusive maximum typical of an amorphous structure. Vacuum annealing of specimens to 773 K significantly changes the diffraction pattern, with sharp peaks now appearing, indicating a crystalline structure (AMC-0).

The behaviour of the mirror specimens under ion bombardment was dramatically different for the crystallized mirrors as compared to the amorphous ones [14]. Bombardment with Ar ions resulted in the development of surface roughness, and a corresponding decrease in reflectivity for the AMC specimens, but had no measurable effect on the AMA specimens, either on microrelief or on the optical properties. Exposure of crystallized specimens to deuterium ions led to the appearance of chipping, and even the destruction

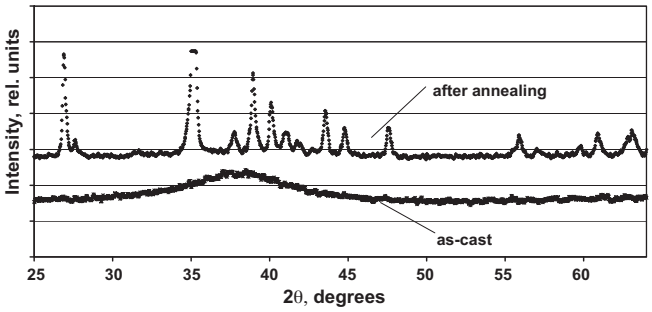

Fig. 1. Results of X-ray diffraction measurements for the specimens AMA-0 (amorphous) and AMC-0 (crystallized by annealing at 773 K for 1 h). Both specimens were machined from the same billet [13].

of one specimen. For the amorphous specimens, only a continuous increase in weight was observed, due to deuterium absorption, again, without change to the optical properties.

Table 1 shows the mass losses observed for one of the crystallized specimens, AMC-1, following various ion exposures. It is noted that all specimens were first cleaned with low-energy deuterium ions (15 min, ion energy 60 eV) prior to any measurements in order to remove the organic film remaining on the surface after polishing and washing. This cleaning procedure is not counted as an exposure.

During the first three exposures to Ar ions, the specimen lost 4.15 mg or about 1.8 μm thickness. During the subsequent 5 exposures to 1 keV deuterium ions, there is a mass loss of ~1.0 mg which would correspond to a decrease in thickness of ~0.42 μm; however, the irregular loss in mass with exposure time indicates other processes are occurring. Following the 9th exposure, to a high fluence of low-energy deuterium ions, there was a mass loss of 2.9 mg, and the specimen surface showed evidence of chipping, see Fig. 2. As seen in the photos, the structure of the chips is typical

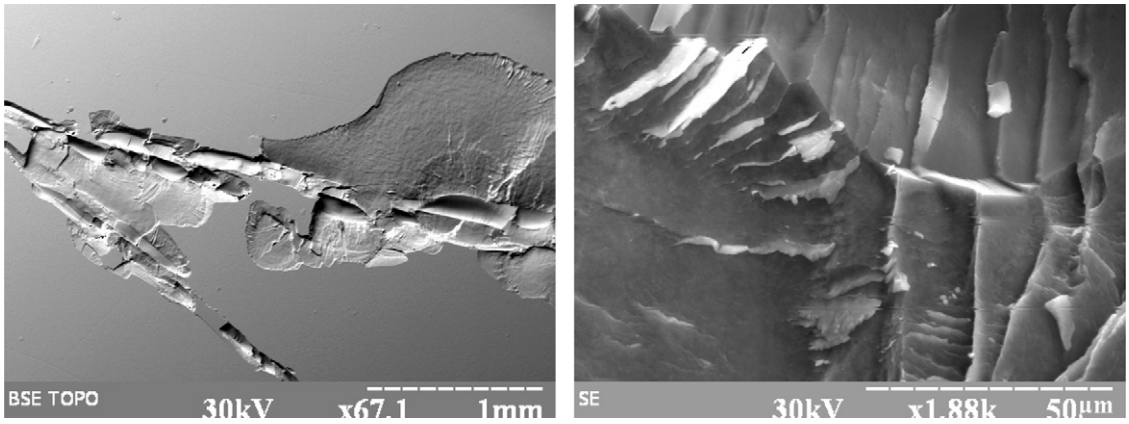

Fig. 2. SEM microphotos of the surface of specimen AMC-1 after the 9th exposure shown in Table 1. Total ion fluence ~2.6×10^{24} ion/m^2.

Table 2
Exposure conditions and weight changes for amorphous (AMA-3) and crystallized (AMC-3) specimens following exposure to 60 eV deuterium ions.

Exposure number	Total exposure time (min)	Total ion fluence (10^{24} ion/m^2)	Weight gain per exposure (μg)	
			AMA-3	AMC-3
1	60	0.47	30	40
2	360	2.82	620	−20 (Chips at edges)
3	660	5.17	920	640
4	960	7.52	820	Destruction of the sample (Fig. 5b)
5	1160	9.09	325	–
6	1460	11.45	825	–
7	1760	13.80	870	–

of brittle failure. Such surface damage was never observed for the amorphous specimens, even with much higher deuterium fluences.

Taking into account that some part of the mass loss is compensated by the mass of absorbed deuterium (more details below), the real thickness of the sputtered layer after exposure 8 might be somewhat larger than 0.42 μm. On the other hand, the large weight loss observed following exposure 7 (560 μg) may also have been caused by the unobserved chipping off of small granules; this may have occurred for other exposures as well. Thus it is very difficult to find an estimate of the sputter layer thickness when specimen is subject to impact of deuterium plasma ions.

The reflectance of specimen AMC-1 was reduced significantly by the Ar ion bombardment, and this was previously attributed to the development of surface roughness [14]. Further exposure of the specimen to 1 keV deuterium ions causes an additional drop in reflectance, see Fig. 3; however, this drop in reflectance was nearly fully restored by subsequent exposure to 60 eV deuterium ions (9th exposure in Table 1). This suggests a chemical process similar to that observed for Be [16,17] and Al [18] mirror specimens, where a decrease in reflectance was interpreted as being due to an increase in thickness of an oxide/hydroxide surface layer. The inability of the low-energy deuterium ions to restore the initial (prior to Ar ion exposure) reflectance of this particular specimen confirms that the Ar ions did lead to an increase in surface roughness.

The similarity of the changes in reflectance in response to high energy deuterium impact (drop in reflectance) and low energy deuterium impact (recovery of reflectance) to that of Be [16,17] and Al [18] mirrors is consistent with SIMS results which indicate that BeO is the main constituent of the surface oxide layer, see Fig. 4a. Moreover, SIMS depth profiles for amorphous specimens following bombardment with deuterium plasma ions of different energies change in a manner very similar to that observed for Be specimens, i.e, the oxidized layer thickness increases following exposure to keV energy ions and decreases following exposure to low energy ions (~60 eV), Fig. 4b. We note that these SIMS

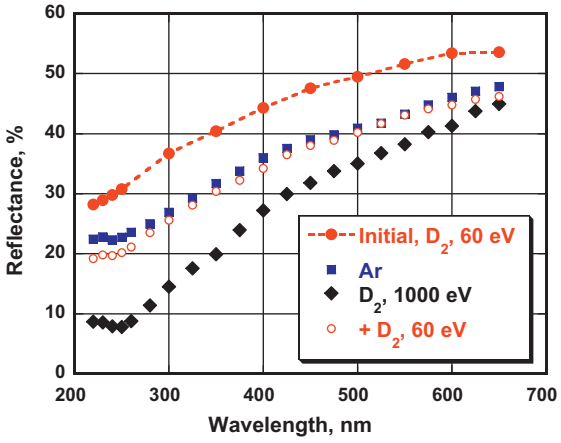

Fig. 3. Spectral reflectance of a crystallized specimen (AMC-1) measured prior to the first exposure to Ar ions (dotted line), after the third exposure (blue squares), and after the eighth (rhombuses), and the nineth (small red circles) when the chips shown in Fig. 2 have appeared on the surface.

measurements were carried out with specimens of a slightly different composition than those studied in the present paper: Zr(46.75)Ti(8.25)Cu(7.5)Ni(10)Be(27.5). We also realize that the (unknown) relative sensitivities of the various oxides in the SIMS measurements make this conclusion tentative. However, this result is in a qualitative agreement with data of XPS (X-ray photoelectron spectroscopy) measurements on specimens with a similar composition [19]. The authors of that paper have found that the uppermost oxide film mainly composed of BeO, in spite of the Be portion in the bulk of the material is less than 30%.

In Table 2 we outline the deuterium exposure conditions and observations for the pair of specimens AMA-3 (amorphous) and AMC-3 (crystallized) fabricated from the same billet. Following the

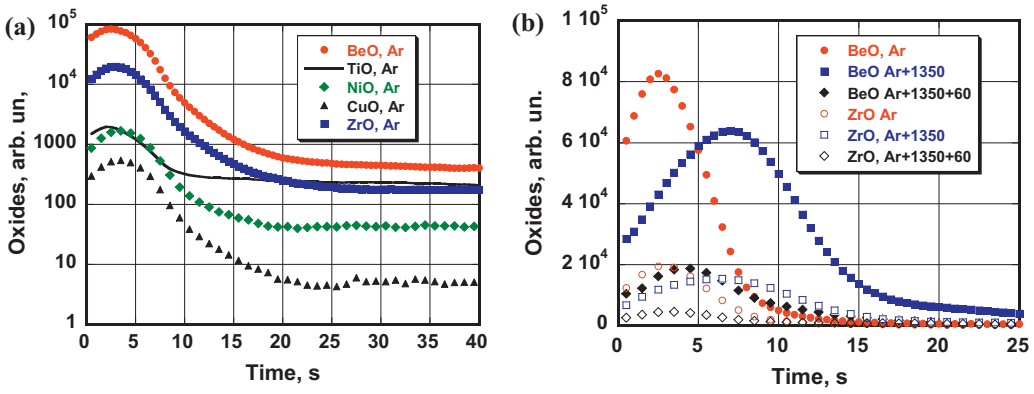

Fig. 4. (a) – SIMS profiles of various metal oxides from the surface of an AMA specimen following exposure in DSM-2 to 1 keV Ar ions to a fluence of 1.9×10^{24} ion/m^2 for cleaning samples from contaminants; (b) – SIMS profiles of BeO and ZrO: circles – after cleaning specimen with Ar ions, squares – after cleaning and bombardment with deuterium plasma ions of 1350 eV energy, rhombuses – after additional exposure to deuterium plasma ions with energy 60 eV; solid points – for BeO and open – for ZrO.

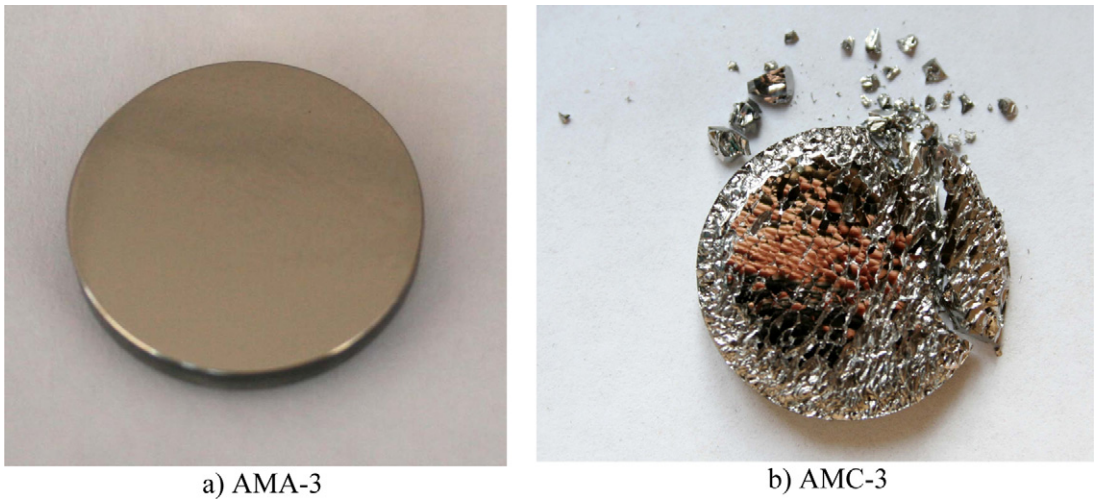

Fig. 5. Photos of $Zr_{41.2}Ti_{13.8}Cu_{12.5}Ni_{10}Be_{22.5}$ specimens following exposures to low-energy (60 eV) deuterium ions to a fluence of 7.5×10^{24} ions/m^2: (a) – amorphous sample AMA-3 (b) – crystallized sample AMC-3.

initial cleaning, the specimens were subjected to 7 exposures to 60 eV deuterium ions at an ion current density of $j = 20.9$ A/m^2.

After the 4th exposure, and a total ion fluence of 7.5×10^{24} ions/m^2, the crystallized specimen was found to have undergone a catastrophic destruction (see Fig. 5b). For comparison, the amorphous specimen is shown, as it appeared following the same exposure (in Fig. 5a). Further exposure of specimen AMA-3 to a total fluence of 14×10^{24} ions/m^2 did not lead to any visible changes in the mirror surface.

As indicated in Table 2, the amorphous specimen experienced a continuous increase in mass when exposed to the low energy deuterium ions. The mass changes for this specimen, and also for specimen AMA-1, are plotted in Fig. 6 showing a good agreement to a linear fit. It should be noted that specimen AMA-1 twice experience short exposures to 1 keV deuterium ions; the 1st and 6th exposures; all others were at 60 eV. Following the 6th exposure, the specimen experienced a small mass loss (see Fig. 6), as compared to the situation following the 5th exposure. This indicates that the mass loss due to sputter erosion by the 1 keV ions is greater than the mass gain due to deuterium uptake.

Assuming all of the weight gain is due to the uptake of deuterium (and negligible erosion) and D_2^+ ions as the main ion component in a ECR plasma [20], the data in Fig. 6 corresponds to a uniform retention of ~13% of the incident deuterium flux. In an earlier study [13], it was found for specimens of similar composition produced by Liquidmetal Technology Corporation (USA) that the uptake deuterium fraction increased approximately linearly with ion energy; from ~5% at 20 eV to ~12% at 100 eV. So, the 13% uptake for 60 eV ions found in the current study can be considered as very similar.

Laser ablation time-of-flight mass spectrometry (LA-TOF-MS) was also used to measure the comparable deuterium content of two of the specimens, AMA-3 and AMA-7. The ion exposures experience by AMA-3 are given in Table 2 and shown in Fig. 6, while AMA-7 was exposed to a total ion fluence of 1.73×10^{24} ions/m^2, with the majority, ~92%, at energy 60 eV and the remainder at 1.35 keV. The total increase in mass for AMA-7 was 220 μg, or about half of the mass increase experienced by specimens AMA-1 and AMA-3 for the same ion fluence (see Fig. 6), and more than an order of magnitude less than the total mass gain of these specimens. Each specimen experienced 22 successive laser pulses on the same spot. The diameter of the spot was 300 μm, the pulse duration 40 ns, and the laser beam power ~10^9 W/cm^2 at the wavelength 680 nm. With each laser pulse the layer of ~1.2 μm in thickness was evaporated. After 22 laser pulses, the crater depth was ~26 μm for both specimens. An example of the mass spectrum taken of the released gases during the 10th laser pulse for specimen AMA-3 is shown in Fig. 7. Qualitatively similar spectra were observed for each laser pulse, with no trend to less D being released with increasing depth. This tells us that the deuterium penetration into the specimen goes well beyond the ion implantation depth (few nm for 60 eV D^+ ions).

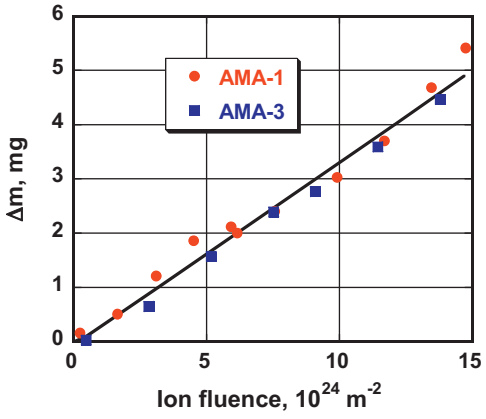

Fig. 6. Ion fluence dependence of the integrated weight gain (the sum of all previous weight increases) for amorphous specimens AMA-1 and AMA-3.

4. Discussion

In previous experiments with the DSM-2 plasma exposure facility where mirror specimens (Be [16,17], Al [18] or amorphous [14]) were exposed to low-energy ions extracted from a deuterium plasma (≤60 eV), the increase in thickness of surface oxide layers has never been observed. On the contrary, when thick oxide/hydroxide layers existed on specimens, the layer would be reduced in thickness by the low-energy deuterium ion exposure. This cleaning process is also observed in the current experiment through the restoration of reflectance following the drop in reflectance caused by the exposure to 1.35 keV ions, see Fig. 3. Therefore, the gain in weight experienced by the specimens is attributed exclusively to the absorption of deuterium.

When comparing data on deuterium absorption by Zr-based amorphous alloys, it is important to note whether hydrogenation is done electrochemically, by ion implantation, or from the gas phase. In the latter case, the very important role of gas–surface

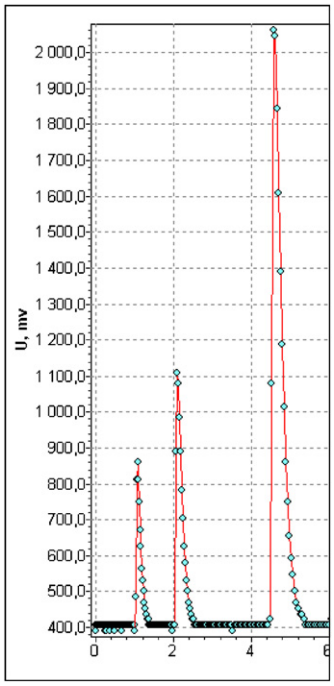

Fig. 7. Mass spectrum of ablated material from the 10th laser pulse for sample AMA-3 after exposures in deuterium plasma up to ion fluences 13.8×10^{24} ion/m^2.

interactions must be taken into account [21], while for ion implantation, the surface interface has a much smaller effect. With electrochemical hydrogenation, the role of the surface differs significantly, but the process may still be affected by the existence of surface oxide layers. To decrease the effect of oxides, Pd coatings are frequently used [e.g., 22] resulting in hydrogen atoms being able to diffuse through the surface more freely. Similar coatings are also used in gas-phase experiments [23].

In Ref. [24], the electrochemical hydrogenation procedure was applied to an amorphous specimen of the same composition as used in the current study. By taking into account the specimen dimensions, charging time and current density, and the final hydrogen-to-metal ratio, H/M ~ 0.92, we calculate that the absorbed hydrogen fraction was ~1%. This is much lower than our value of 13%, however, our average H/M ratio is also much lower. For the maximum weight gain of our amorphous specimens, ~5 mg (Fig. 5) and for a specimen mass of ~8.5 g, the average D/M ratio is ~0.018. Thus in our case it appears that we are far from approaching saturation, although we do not have reliable information on the depth distribution of the deuterium in our specimens.

Our experiments have indicated significant differences in hydrogen absorption behavior for amorphous and crystalline specimens. In Ref. [25], the authors find a characteristic scale length for short range order in similar V1 alloys to be 1.5–3 nm. A similar size (0.5–2 nm) was found for medium range order zones in $Ti_{60}Zr_{15}Ni_{15}Cu_{10}$ amorphous alloy [26]. Furthermore, no change was observed in either the size or the density of the zone during hydrogenation, up to H/M ≈ 1.4. This led to the conclusion that hydrogenation did not affect the structure of the material, and that it remained amorphous [26].

Recrystallization does radically alter the structure of the material. In our experiments it was not possible to identify peaks on the X-ray diffraction spectrum (Fig. 1) of the recrystallized material. However, our spectrum is very similar to those observed in Refs. [27,28] for an identical amorphous material; this despite differences in recrystallization temperature and time: 673 K and 15 h in Ref. [27], 633 K and 1 h [28] and 773 K and 1 h in our experiment. Thus we assume that the primary characteristics of the structure following crystallization are similar; in particular, Be_2Zr [26] and Zr_2Cu crystals have been identified. Thus, the crystallization process changes the material from uniform structure and composition, to non-uniform composition and structure.

In the review [29], it was reported that greater mobility and lower activation energies for diffusion were found in glassy materials, provided H/M > 0.01. Given similar rates of hydrogen uptake observed for the amorphous and recrystallized materials in our study, we thus speculate that the D concentration was much higher in the surface region exposed to the plasma ions for the crystallized specimens. This would lead to higher near-surface concentration of D, and consequently, large stresses leading to cracking and fracturing. Hydrogen embrittlement of Zr-based alloys is a well-known phenomenon [9]; if the hydrogen concentration exceeds the solubility limit at a given temperature, zirconium and titanium hydride phases appear. The accompanying volumetric changes result in the formation of microcracks along grain boundaries [9]. In contrast, hydrides were not found in an identical amorphous alloy (V1) following long hydrogen charging by using X-ray diffraction and transmission electron microscopy [28].

5. Conclusions

A comparison has been made of the effects of deuterium plasma exposure on crystalline and amorphous mirrors of $Zr_{41.2}Ti_{13.8}Cu_{12.5}Ni_{10}Be_{22.5}$. For ion fluences as low as $\sim 6 \times 10^{24}$ D/m^2, the crystalline specimens suffered serious damage, including the complete disintegration of one specimen. However, mirrors in the amorphous state did not show any visible changes, even at much higher fluences. Hydrogen embrittlement is a well-known property of Zr-based alloys, and the difference in the behavior of the amorphous and crystalline specimens is thought to be related to the relative ease of hydrogen transport through the amorphous material, as compared to the crystalline material. This would lead to much higher D concentrations in the near surface of the crystalline specimens, and ultimately brittle destruction.

This work has shown that while this amorphous material may have some favorable properties with regard to erosion due to charge-exchange atoms, there is a critical difficulty with the possibility of recrystallization leading to significantly reduced performance. This may rule out the use of the current alloy in large scale fusion experiments, but we hope that in the near future new amorphous alloys might be developed with a greater resistance to recrystallization.

Acknowledgement

Part of this work, supported by Canadian Government, was carried out within the framework of the STCU project #3668.

References

[1] W.L. Johnson, Mater. Res. Soc. Bull. 24 (1999) 42–56.
[2] W.H. Wang, C. Dong, C.H. Shek, Mater. Sci. Eng. R Rep. 44 (2004) 45–89.
[3] A. Inoue, X.M. Wang, W. Zhang, Adv. Mater. Sci. 18 (2008) 1–9.
[4] M.F. Ashby, A.L. Greer, Scripta Mater. 54 (2006) 321–326.
[5] A. Inoue, Acta Mater. 48 (2000) 279–306.
[6] W.L. Johnson, JOM Journal of the Minerals, Metals and Materials Society, 2002, March, p. 40.
[7] A. Inoue, A. Takeuchi, Mater. Sci. Eng., A 375–377 (2004) 16–30.
[8] Daewoong Suh, R.H. Dauskardt, Scripta Mater. 41 (2000) 233–240.
[9] N.M. Vlasov, I.I. Fedik, Met. Sci. Heat Treat. 45 (2003) 328–331.
[10] V.S. Voitsenya, A.F. Bardamid, M.F. Becker, et al., Rev. Sci. Instrum. 70 (1999) 790–793.
[11] R. Behrisch, G. Federichi, A. Kukushkin, et al., J. Nucl. Mater. 313–316 (2003) 388.
[12] A.F. Bardamid, A.I. Belyaeva, V.N. Bondarenko, et al., Phys. Scripta T123 (2006) 89–93.

[13] V.S. Voitsenya, A.S. Bakai, A.F. Bardamid, V.G. Konovalov, et al., J. Plasma Fusion Res. Ser. 8 (2009) 1379–1384.
[14] V.S. Voitsenya, A.F. Bardamid, A.I. Belyaeva, et al., Plasma Devices Opers. 17 (2009) 144–154.
[15] A.F. Bardamid, V.T. Gritsyna, V.G. Konovalov, et al., Surf. Coat. Technol. 103–104 (1998) 365–369.
[16] V.S. Voitsenya, A.F. Bardamid, A.I. Belyaeva, V.G. Konovalov, D.V. Orlinskij, I.V. Ryzhkov, A.N. Shapoval, A.F. Shtan', S.I. Solodovchenko, K.Yu. Vukolov, J. Nucl. Mater. 329–333 (2004) 1476–1480.
[17] A.F. Bardamid, V.N. Bondarenko, J.W. Davis, V.G. Konovalov, O. Litvin, I.V. Ryzhkov, A.N. Shapoval, A.F. Shtan', S.I. Solodovchenko, V.S. Voitsenya, J. Nucl. Mater. 405 (2010) 109–117.
[18] A.F. Bardamid, A.I. Belyaeva, J.W. Davis, M.V. Dobrotvorskaya, A.A. Galuza, L.M. Kapitanchuk, V.G. Konovalov, I.V. Ryzhkov, A.F. Shtan', K.A. Slatin, S.I. Solodovchenko, V.S. Voitsenya, J. Nucl. Mater. 393 (2009) 473–480.
[19] M. Kiene, T. Strunskus, G. Hasse, F. Faupel, Mater. Res. Soc. Symp. Proc. 554 (1999) 167–172.
[20] K.S. Golovanivsky, V.D. Dugar-Jhabon, V.D. Shchepilov, et al., Sov. J. Plasma Phys. 7 (1981) 324.
[21] CHENG. Xiao-ying, W.A.N.G. Fang, Trans. Nonferrous Met. Soc. China 19 (2009) 377–382.
[22] D. Zander, E. Tal-Gutelmacher, L. Jastrow, U. Koster, D. Eliezer, J. Alloys Compounds 356–357 (2003) 654–657.
[23] V.T. Huett, D. Zander, L. Jastrow, E.H. Majzou, K.F. Kelton, U. Köster, J. Alloys Compounds 379 (2004) 16–22.
[24] Delin Peng, Jun Shen, Jianfei Sun, Yuyong Chen, J. Mater. Sci. Technol. 20 (2004) 157–159.
[25] A.S. Bakai, I.M. Mikhailovskij, T.I. Mazilova, Low Temperat. Phys. 28 (2002) 279–283.
[26] X.Q. Guo, D.V. Louzguine, S. Yamaura, L.Q. Ma, W. Sun, M. Hasegawa, A. Inoue, Mater. Sci. Eng. A 338 (2002) 97–100.
[27] M.-P. Macht, N. Wanderka, Q. Wei, I. Sieber, N. Deyneka, Mater. Sci. Eng. A 304–306 (2001) 701–705.
[28] D. Suh, R.H. Dauskardt, Mater. Sci. Eng. A 319–321 (2001) 480–483.
[29] N. Eliaz, D. Eliezer, Adv. Perform. Mater. 6 (1999) 5–31.